Quantum statistical effects in nano-oscillator arrays

Douglas M. Photiadis,* J. A. Bucaro, and Xiao Liu
Naval Research Laboratory, 4555 Overlook Avenue SW, Washington, DC 20375-5320, USA
(Received 20 April 2005; revised manuscript received 3 March 2006; published 14 April 2006)

We consider a large, free-standing array of coupled, planar oscillators each several hundred nanometers on a side fabricated from a single layer of dielectric. In particular, we predict the low-temperature heat capacity and Brillouin-scattered cross section based upon a numerical calculation of the density of states (DOS) for this nanostructured array. The DOS, which is interesting in its own right, is found to have an average value nearly independent of frequency and a number of gaps of varying depths. The predictions suggest that it should be possible to use low-temperature measurements of the Brillouin cross section and/or the specific heat to observe the quantum statistics obeyed by various rigid-body modes of the array, some of which involve the center-of-mass motion of a large number of atoms. As such, these measurements would result in a considerable extension of the domain in which quantum mechanics has been tested.

DOI: 10.1103/PhysRevB.73.165314 PACS number(s): 85.85.+j

I. INTRODUCTION

Over the past decade, significant effort has been focused on the observation of quantum effects in large systems, both to test quantum mechanics in this regime and to directly observe quantum decoherence phenomena arising from coupling to the environment. Mechanical oscillators have often been considered in this context because displacement states of the oscillator can serve as "Schrödinger cat" states in the investigation of these phenomena. The measurement concepts reported to date in this area[1–5] have primarily involved investigating the quantum properties of a single oscillator, though short linear chains of coupled oscillators have been considered recently in the context of minimum thermal conductance[6] and entanglement.[7] Concepts involving a mechanical oscillator coupled to the optical modes of a cavity have been considered by Bose *et al.*,[8] while the investigation of a mechanical oscillator coupled to the electrons in a Cooper pair box,[9] the electronic analogy, is under way. Recent experimental results have pushed close to the limits of the uncertainty principle.[10]

A different approach, and the central focus of this paper, is to explore the extent to which one can probe the quantum behavior of mechanical oscillators by observing the bulk properties of a large, free-standing array of coupled nano-oscillators; i.e., by investigating a phononic crystal with structure at nanometer length scales. Our principal results are theoretical predictions for two such quantities, the specific heat and the Brillouin spectra, both of which have in the past provided experimental evidence for the quantum behavior of solids at low temperatures.

Bulk statistical measurements at low temperatures provide more limited tests of quantum mechanics than do direct measurements of quantum interference.[8,10] Nevertheless, the measurements considered here enable one to verify that the relevant modes, modes involving macroscopic whole-body motion of individual nano-oscillators in the geometry we consider, obey quantum statistics and therefore have quantized energy levels. This information is contained in the temperature dependence of the specific heat and Brillouin-scattered power at low temperatures.

The system we consider is a free-standing, periodic, planar structure as shown in Fig. 1. The system is assumed to be monolithic, fabricated from a single layer of silicon or diamond for example. The particular dimensions have been chosen so that modes associated with rigid-body motion of an individual oscillator will be in a quantum regime, $\hbar\omega \sim k_b T$, at a reasonable temperature $T \sim 20$ mK.

The classical solution for the eigenfunctions and the spectrum is central to the quantum behavior of the system, the density of states directly determining the specific heat[11] and, in conjunction with the polarization of the modes, also determining the Brillouin-scattered power levels. Since our principal aim is to investigate the quantum behavior of the system, we focus on the low-temperature behavior of these quantities, and thus on the low-frequency states. We therefore proceed directly to a determination of the classical normal modes of the system in Sec. II.

In Sec. III, the specific heat for the system is obtained using the computed density of states (DOS). It is shown that the specific heat varies in a nominally linear fashion with temperature because of the two-dimensional character of the system at fairly low temperatures $T \lesssim 5$ K for the structure we have considered. The nanostructure of the system is shown to give rise to a peak in c_v/T at very low temperatures $T \sim 10$ mK, with the onset of the peak beginning at about 100 mK.

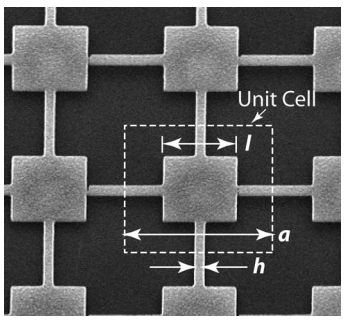

FIG. 1. Geometry of a free-standing nano-oscillator structure. The values used for calculations are $l=200$ nm, $a=360$ nm, $h=20$ nm, thickness $\delta=20$ nm, and material parameters of Si.

In Sec. IV, the cross section for Brillouin scattering from the system is predicted. The Brillouin-scattering cross section is shown to dominated by the ripple of the film, as opposed to volume scattering, and the magnitude of the scattering is given in terms of the spectra and eigenfunctions of the system. Finally, we give estimates for the order of magnitude of these effects at low temperatures, and the potential for these measurements to be employed in the search for quantum effects in nano-oscillator systems. We have found that observing the predicted quantum effects requires very sensitive measurements, but attaining this precision is certainly not far beyond our current capability.

II. THE CLASSICAL SPECTRUM

The phonon modes of the nanoarray are modeled using continuum three-dimensional (3D) elasticity theory, an approach known to give a good approximation to the vibrational spectra of bulk solids for frequencies well below the edge of the Brillouin zone.[12] The Lagrangian is therefore given by[13]

$$L = \frac{1}{2}\int_V dV\{\rho\vec{v}^2 - \sigma_{ij}u_{ij}\} \tag{1}$$

with $u_i(x)$ the displacement field, $v_i(x)=\dot{u}_i(x)$ the velocity field, $u_{ij}(x)=(1/2)(\partial u_i/\partial x_j+\partial u_j/\partial x_i)$ the strain tensor, $\sigma_{ij}(x)$ the stress tensor, and ρ the density. The integration is restricted to the volume of the sample and stress-free boundary conditions ($\sigma_{ij}=0$) are imposed on the free surfaces of the system. We assume, for simplicity, that the material is isotropic. This assumption, while not valid for single-crystal films, will have a weak effect on the quantities we consider here, the specific heat and the Brillouin-scattered power levels.

A. Modes of an isotropic plate

The solutions of the boundary value problem for the free-standing array are superpositions of the wave solutions of a uniform thin film, and it is useful to recall the nature of these solutions before examining the numerical results. The symmetry of the system with respect to reflections in z, together with translation invariance in the xy plane, imply that the waveguide solutions of the plate are of the form $u_i(x_\perp,z;k_\perp)=g_i(k_\perp,z)\exp(ik_\perp\cdot x_\perp)$, where the function $g_i(k_\perp,z)$ is even or odd in z. The cutoff frequency for the first higher-order waveguide mode is given by[14]

$$\omega_c = \pi c_s/\delta, \tag{2}$$

where c_s is the velocity of shear waves in the bulk medium and δ is the sample thickness. The wave types can be further classified by their polarization as symmetric dilatational or compressional modes, symmetric shear horizontal modes, and antisymmetric flexural modes. Auld[14] gives an excellent and thorough discussion of the properties of the waveguide modes.

The highest frequency we have considered for the system shown in Fig. 1 ($\delta=20$ nm, $c_s=5\times10^3$ m/s) is $f=35$ GHz, well below the lowest cutoff frequency $f_c\approx125$ GHz, and therefore the relevant modes of the system are the solutions below cutoff. In this frequency range, one mode of each wave type survives for a given transverse wave number $k_\perp$, and the z dependence of the modes becomes trivial; i.e., independent of z for the symmetric case and simply proportional to z for the antisymmetric case. The polarization of the modes, the direction of the particle velocity, also becomes trivial: the polarization of the antisymmetric mode is normal to the film, out of plane; the polarization of the shear horizontal mode is transverse to the direction of propagation and in the plane of the film; and the polarization of the longitudinal mode is in the direction of the wave propagation, also an in-plane mode. The dispersion relations also simplify below the cutoff frequency; the symmetric modes are similar to their counterparts in a bulk medium, while the antisymmetric, flexural mode departs substantially from any 3D analog and exhibits strong dispersion, behaving approximately as $\omega\propto k^2$ as $\omega\to0$, a dramatic slowing. This dependence underlies the unusual low-frequency scaling behavior of the density of states and the corresponding low-temperature behavior of the specific heat.

In the frequency range $\omega\leqslant\pi c_s/(3\delta)$, Mindlin's thick plate theory[15] provides a good approximation to the flexural wave dispersion relation, while leading-order thin plate theory, due originally to Kirchhoff,[16] yields reasonable results in this frequency range and becomes accurate for $\omega\leqslant\pi c_s/(10\delta)$. The dispersion relation for the antisymmetric flexural wave in the thin plate theory approximation is[17]

$$\omega = (D/m)^{1/2}k^2 \tag{3}$$

with $D=E\delta^3/(1-\nu^2)$ the flexural rigidity (here E and ν are the Young's modulus and Poisson ratio, respectively) and $m=\rho\delta$ the mass per area of the plate. The dispersion relation for the shear mode is simply $\omega=c_sk$, while the dispersion relation for the compressional wave is $\omega=c_pk$ with $c_p=E/\rho(1-\nu^2)$, similar to the bulk medium result. The ratio of the flexural and compressional wave speeds is easily estimated from Eq. (3) to be $c_f(\omega)/c_p=\omega\delta/c_p\ll1$; hence the wave speed of the antisymmetric flexural wave is always far less than the wave speed of the symmetric modes. We will use these expressions to obtain simple formulas for the DOS and specific heat of a uniform, isotropic plate to better understand our numerical results.

B. Modes of the nano-oscillator array

We follow the analysis approach employed by Lazarenkova and Balandin.[12] The normal modes are calculated by seeking solutions of the Bloch form $u_i(x_\perp,z)=\exp(ik_\perp\cdot x_\perp)U_i(x_\perp,z)$ to the equations of 3D elasticity theory. Here $x_\perp=(x,y)$ and $k_\perp=(k_x,k_y)=(2n\pi/L_x,2m\pi/L_y)$ are in the plane of the system, and $U_i(x_\perp,z)$ is taken to be periodic in the xy coordinates. The quantities n and m are integers, L_x and L_y are the dimensions of the crystal, and the boundary conditions at $(x,y)=(\pm L_x/2,\pm L_y/2)$ are taken to be periodic, an approximation which will not be significant for a large system. This results in a Hermitian boundary

value problem in the unit cell which yields the resonance frequencies for a particular wave number, with one eigenfrequency for each subband of the spectrum.

The system is still symmetric with respect to reflections in the z direction, and therefore the even and odd solutions are uncoupled by the imposition of the boundary conditions. The resulting solutions can thus still be classified as quasiflexural, quasishear, or quasilongitudinal. Further, in the frequency range of interest, as pointed out in the previous section, Mindlin plate theory provides accurate solutions. This fact can be employed to achieve considerable computational savings, since plate theory is a 2D rather than a fully 3D model. Within this approach, the symmetric and antisymmetric solutions are obtained separately.

The computation was done using the commercial numerical package FEMLAB, which enables solutions in the context of both 2D and 3D models. Solutions were first obtained for several representative wave numbers using 3D elasticity theory. A sufficiently fine grid was used in the calculation to ensure that the errors in the resonance frequencies at the high-frequency end of the calculation were always smaller than 5%, with much smaller errors at lower frequencies. This solution of course contains both symmetric and antisymmetric modes. Separate 2D models were then used to obtain the solutions; the same accuracy was achieved with more than an order of magnitude savings in the computation time required. The boundary value problem was then solved at $(N/2)\times(N/2)=1600$ distinct wave numbers in the first Brillouin zone, a computation requiring about 24 h on a desktop computer. Here N^2 is the total number of unit cells in the array and gives the size of the system; provided N is large enough so that discretization effects in wave number space are unimportant, the results depend on N in a trivial manner.

Figure 2 shows the calculated dispersion surfaces, the Bloch subbands, of the nano-structured array for frequencies below 5 GHz. The smoothness of the dispersion surfaces shows that the sampling in k space is sufficient and also demonstrates the numerical stability of the calculations. Figure 2(a) shows the dispersion surfaces for the antisymmetric (with respect to z), out-of-plane modes, while Fig. 2(b) shows the dispersion surfaces for the symmetric, in-plane modes. We present these results separately because the two sets of modes are quite different and later, we shall need the out-of-plane density of states to predict the Brillouin scattering from the system.

Comparing Figs. 2(a) and 2(b), the overall slowness of the out-of-plane modes (small values of $\partial\omega/\partial k$) relative to the in-plane modes, and their resulting dominance in the density of states, is apparent. This property of the spectrum is due to the slowness of flexural waves relative to shear and compressional waves in a uniform medium as discussed in the previous section. The exceptions to this behavior are the narrow subbands in the in-plane spectrum near 1 and 4.5 GHz. The effective stiffness of these modes is predominantly associated with flexure of the square "legs" (20×20 nm^2) between each "paddle," and thus the strain field in these modes is also predominantly flexural despite involving displacements in the plane of the array system.

The states in the low-frequency subbands extending up to about 1 GHz involve whole-body motion of significant portions of the nano-oscillator elements, the paddles. The first quasigap in the spectrum, a gap in the out-of-plane spectrum, is associated with weakly coupled local 1-1 modes of the paddles (the nearly horizontal surface at $\approx$2.25 GHz), and occurs in the range from 1 to 2 GHz. These modes may be considered to be analogous to the optical modes of a crystal, but they arise from the nanostructure of the system rather than internal vibration in the unit cell. The low-frequency modes are the most interesting with regard to testing the limits of quantum mechanics[18] and environmentally induced decoherence,[19,20] because the associated energy eigenstates exhibit coherent center-of-mass motion of large numbers of atoms; in the geometry considered a single nano-oscillator contains $\sim 4\times 10^7$ Si atoms. Coherent motion of a 1000×1000 array would involve 10^{13} atoms, a nearly macroscopic phenomenon.

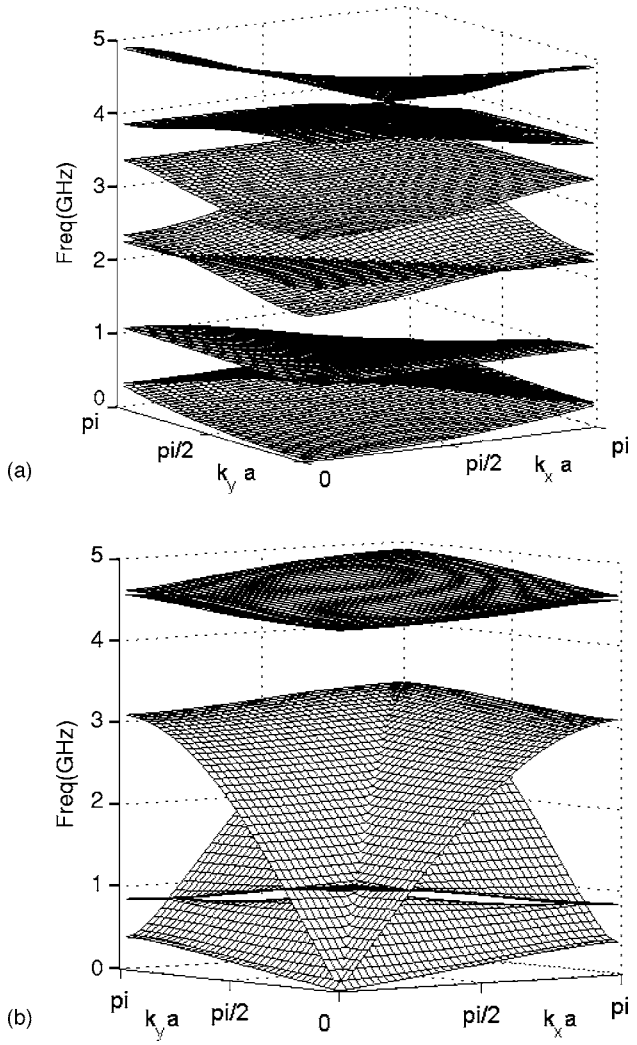

FIG. 2. Numerically calculated dispersion surfaces of the nanostructure in ω-k space: (a) out-of-plane and (b) in-plane modes.

C. Density of states

The DOS is obtained in a straightforward fashion from the dispersion surfaces by integrating over an appropriate

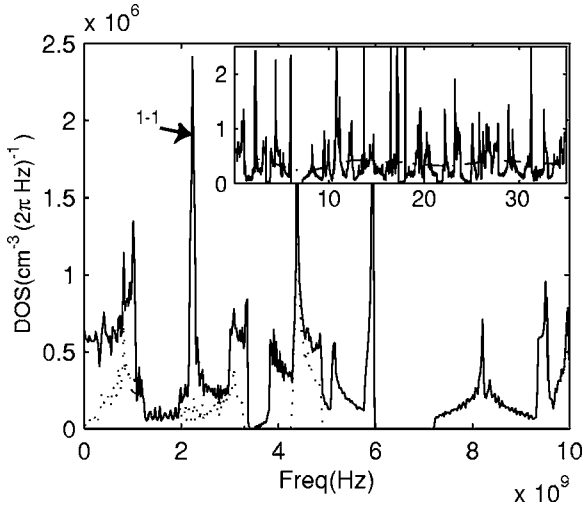

FIG. 3. Numerically calculated phonon DOS of the nanostructure:—total; ···out-of-plane. The inset shows the DOS over the band 0–35 GHz:—total;--average.

bandwidth. We found a bandwidth $B=25$ MHz resolved the various resonance peaks in the DOS, and yet was still large enough that the discretization in the states caused by the finite system size did not produce significant "numerical noise" in the results—typical level spacings due to the finite structure size were at most 4 MHz. Singularities near the band edges can of course not be fully resolved in this manner.

The numerically computed density of states is shown in Fig. 3. The quasigap in the spectrum in the range from 1 to 2 GHz can be clearly seen, while a true gap appears in the spectrum at approximately 6 GHz. The 1-1 collective mode, singled out in the figure, is the dominant low-frequency resonance of the nanoarray. The in-plane contribution to the DOS is shown in the figure by the dotted line. The dominance of the flexural modes in the DOS is apparent, with the in-plane contribution being small except near the flexural resonances. The one exception to this behavior is the peak near 3 GHz which is due to the band edge of the shear modes.

A notable feature of the results is that the average DOS (the dashed line in the inset) is more or less constant in this frequency range. We point out this behavior because the frequency dependence of the DOS directly determines the temperature dependence of the specific heat (and other physical quantities). This frequency independence results from the dispersive properties of the flexural modes which dominate the spectrum. Indeed, using the results from Sec. II A, the DOS of a flexural wave system of size L^d in d dimensions may be shown to be

$$N(\omega) = \frac{(\omega L/2c_f)^d}{\pi^{d/2}\Gamma(d/2)\omega} \overset{d\to 2}{=} \frac{L^2}{4\pi}(m/D)^{1/2} \tag{4}$$

and is independent of frequency in two dimensions,[21] in accord with the average DOS shown in Fig. 3. This approach underestimates the DOS of the nanostructure considered by a factor of about 2, primarily because of the in-plane flexural modes which cannot be taken into account in this fashion. The dispersion of the neglected modes is, however, the same as that of the flexural plate modes, and thus the frequency dependence of the DOS is correctly predicted using this simple formula.

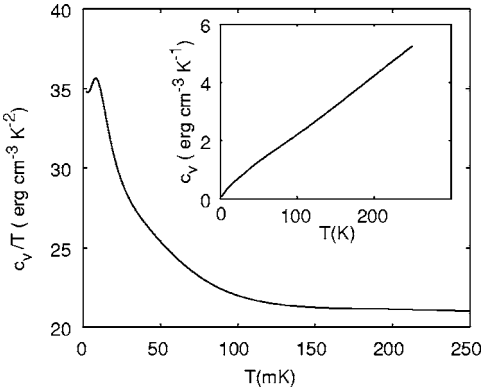

FIG. 4. The ratio c_v/T from Eq. (5) using the numerically computed DOS; c_v is shown in the inset.

III. SPECIFIC HEAT

With the classical modes in hand, the system may be quantized in the usual way,[22] resulting in each normal mode $\omega_{n\lambda}(k)$ being represented by a simple harmonic oscillator degree of freedom with the energy eigenstates $(n+1/2)\hbar\omega_{n\lambda}(k)$. The specific heat at low temperatures may then be obtained exactly as in the case of phonons in a uniform solid[11] with the DOS in that case being replaced by the numerically computed DOS for the phononic crystal we have considered,

$$c_v = \frac{\partial u}{\partial T} = \frac{k_b}{V}\int d\omega\, n(\omega)\frac{e^{x(\omega)}}{(e^{x(\omega)}-1)^2} \tag{5}$$

where $x(\omega)=\hbar\omega/k_bT$. The results for c_v/T and c_v are shown in the temperature range below 250 mK in Fig. 4. In this range the specific heat is reasonably linear, with a low-temperature enhancement in the nominally linear behavior resulting from the nanostructure.

Measurements of the temperature dependence of the specific heat in accord with these predictions would provide evidence that the relevant modes, modes with $\hbar\omega \leqslant 3.5k_bT$, are behaving as simple quantum oscillators obeying Bose statistics. Modes in the lowest-frequency band, and the associated peak in the DOS at the band edge, give rise to the peak in the c_v/T plot at about 10 mK, and provide a clear signature of the quantum behavior of these states—recall that these modes are locally whole-body modes of the nano-oscillators.

The near linear behavior of the specific heat results from the roughly constant DOS at low frequencies and differs from the T^2 dependence[23] typically assumed for 2D phonon systems. This overall temperature dependence is thus due to the two-dimensional nature of the system as opposed to the nanostructure. In d dimensions, using Eq. (4) for the DOS of a uniform flexural system in the basic expression for the specific heat, Eq. (5), one may show that,

$$C_v \approx k_b \frac{L^d}{2^d}\left(\frac{m^{1/2}k_bT}{D^{1/2}\pi\hbar}\right)^{d/2}\frac{d}{2}\left(\frac{d}{2}+1\right)\zeta(d/2+1) \qquad (6)$$

at low temperatures. Here, ζ is the Riemann zeta function. In 1D, the heat capacity varies as $T^{1/2}$, while in 2D the predicted temperature dependence is T, as we have found above. This behavior should set in at temperatures such that the higher-order waveguide modes are frozen out, $3.5k_bT < \hbar\pi c_s/\delta$, where we have used Eq. (2) for the lowest cutoff frequency of the film. For 20 nm Si, this yields $T \lesssim 6$ K, a modest temperature. This behavior has not yet been observed but could certainly be investigated by making measurements on uniform free-standing films.

Finally, assuming a constant DOS n in accord with the numerical results in two dimensions, one finds $c_v = k_b(3.3k_bT/\hbar)n$. Therefore, in addition to extending the domain in which quantum mechanics has been tested, such specific heat measurements directly measure the DOS of thin-film-based nanostructures, provided the DOS is dominated by the flexural degrees of freedom considered here.

IV. BRILLOUIN SCATTERING

The quantum statistics of a nano-oscillator array can also be probed in a low-temperature Brillouin-scattering experiment. We follow the usual approach[24–26] and approximate the scattered field due to thermal fluctuations of a nanostructured array by estimating the classical electromagnetic scattering from a coherently vibrating structure, and then replacing the required power spectra of the displacement fields in the classical expressions by quantum expectation values.

A. Classical theory

The scattered vector potential due to an incident electric field $\vec{E}=\vec{E}_0\exp(i\vec{k}_i\cdot\vec{x}-\omega_0 t)$ upon the nanostructure is given in the far field to leading order by[27]

$$A_i(\vec{R},t) \approx \frac{-i\omega_0 e^{i(kR-\omega_0 t)}}{4\pi c^2 R}\int_{V(t)} \chi_{ij}(\vec{x}',t)E_{0j}e^{i(\vec{k}_i-\vec{k})\cdot\vec{x}'}d^3x'; \qquad (7)$$

i.e., a superposition of dipole fields in the usual fashion. The volume $V(t)$ is the scattering volume at time t and $\vec{k}=\hat{R}\omega_0/c$ is the outgoing wave number. To obtain this result, we have assumed the incident field to give rise to a polarization $P_i=\epsilon_0\chi_{ij}E_j$ with χ_{ij} the susceptibility of the system and E_i the total electric field inside the the dielectric. Further, we have replaced the total electric field by the incident field in the integration over the nanostructure, a Born approximation which is reasonable because of the small thickness of the structure. We have also ignored retardation effects because the vibrational frequencies are so small relative to optical frequencies. This approach is similar to that employed by many investigators,[25,28,29] except that we consider the vector potential as opposed to the electric field, and further, we allow the scattering volume to be explicitly time dependent. Our approach is, however, equivalent to that employed in the quoted references and is pursued here only for mathematical convenience.

Brillouin scattering results from volume fluctuations in the susceptibility[30] and, under some circumstances, surface ripple,[31–33] with the relative contribution of surface ripple scattering being determined by the opaqueness of the sample. The volume scattering mechanism is suppressed by a factor of order $(k\delta)^2$ for flexural waves in thin films, the dominant excitations in the case at hand, because of the antisymmetry of the induced polarization across the film. In this case, provided the reflection coefficient is not vanishingly small, the dominant contribution to Brillouin scattering at low frequencies ($f \lesssim 20$ GHz for the geometry considered) arises from ripple scattering, a purely kinematic phenomena. We consider only this mechanism below, and take the susceptability χ_{ij} to be constant.

Only out-of-plane displacements $u_z(\vec{x}_\perp,t)$ need be considered to leading order to compute the ripple scattering, because in-plane motion causes optical scattering only via weak diffractive effects associated with small changes in the spacing of the array. Thus we have from Eq. (7)

$$A_i(\vec{R},t) \approx \frac{-i\omega_0\chi_{ij}E_{0j}e^{i(kR-\omega_0 t)}}{4\pi c^2 R}\int_S d^2x'_\perp \times \int_{u_z(\vec{x}_\perp,t)-\delta/2}^{u_z(\vec{x}_\perp,t)+\delta/2} dz' \exp(-i\vec{q}_\perp\cdot\vec{x}' - iq_z z') \qquad (8)$$

where $q=k-k_i$ is the change in the incident wave number. Changing variables in Eq. (8), $z'=z+u_z(\vec{x}_\perp,t)$, to remove the time dependence of the scattering volume, and assuming the phase shift $k_z u_z(\vec{x}_\perp,t) \ll 1$, we find that the scattered electric field is given to leading order in δ and u_z by

$$\vec{E}(\vec{R},t) \approx k_0^2\delta[\hat{R}\times\hat{R}\times(\chi\cdot\vec{E}_0)]\frac{e^{i(kR-\omega_0 t)}}{4\pi R} \times[a_0(q_\perp) - iq_z u_z(q_\perp,t)]. \qquad (9)$$

Here $u_z(q_\perp,t)$ is the Fourier transform of the out-of-plane displacement field restricted to the illuminated portion of the scattering surface S and

$$a_0(q_\perp) = \int_S d^2x \exp(-i\vec{q}\cdot\vec{x}_\perp) \qquad (10)$$

is a static aperture integral.

The differential cross section, the average power scattered into solid angle $d\Omega$ and frequency interval $d\omega$ divided by the incident power flux, is then obtained by taking the time average of the Poynting vector $\vec{S}=\vec{E}\times\vec{H}$,

$$\frac{d^2\sigma}{d\Omega\, d\omega} \approx \left(\frac{|r(\theta_i)|k_0\sin\psi\cos\theta_i}{2\pi}\right)^2\left(2\pi\delta(\Delta\omega)|a_0(q_\perp)|^2 + \frac{q_z^2}{\Theta}|u_z(q_\perp,\Delta\omega)|^2\right). \qquad (11)$$

where $\Theta\to\infty$ is the time window for the Fourier transform. We have at this point taken the susceptibility χ_{ij} to be isotropic, $\chi_{ij}=\chi\delta_{ij}$, to achieve a simpler result, and have taken

the frequency shifts to be small, $\omega_0/\omega_s=1$. The factor of $\sin^2\psi$ gives the dependence on the polarization of the incident field, $\sin\psi=\hat{R}\times\hat{E}_i$, $r(\theta_i)=-ik\delta\chi/(2\cos\theta_i)$ is the reflection coefficient of the film for incident polarization perpendicular to the scattering plane, and $\Delta\omega$ is the change of the incident frequency. The first term in Eq. (11) gives the Rayleigh-scattering peak while the second term gives the contribution due to scattering from surface ripple.

Checks on Eq. (11) are provided by assuming the nanoarray to be a uniform film. We assume here that the incident field is polarized perpendicular to the scattering plane ($\sin\psi=1$). To check the overall normalization, let us first consider the total cross section for Rayleigh scattering,

$$\sigma_R=\int d\Omega\, d\omega \frac{d^2\sigma_R}{d\Omega\, d\omega}. \tag{12}$$

Provided the surface is large, we have $|a_0(q)|^2 \approx[(2\pi)^2\delta^2(q)]^2\approx A(2\pi)^2\delta^2(q)$. Changing from angular variables to wave number via

$$k_0^2\sin\theta\cos\theta\, d\theta\, d\phi=dk_x dk_y \tag{13}$$

we quickly find the total cross section for Rayleigh scattering to be $\sigma_R=|r(\theta_i)|^2A\cos\theta_i$ in agreement with elementary results.

As a further check, in the case of illumination by a two-dimensional beam of light of width $2L$ incident upon the film at angle θ in the xz plane, we may quickly find from Eq. (9) the scattered electric field in the specular direction,

$$|E|=\frac{|r(\theta_i)\cos\theta_i k_0E_0a_0(0)|}{2\pi R}=\frac{r(\theta_i)k_0L|E_0|}{\pi R}=r(\theta_i)I_0^{1/2}, \tag{14}$$

and the scattered intensity $I_Q=|E_Q|^2$ from an assumed sinusoidal velocity field $\xi_0\cos(Qx-\omega_s t)$,

$$I_Q=I_0|r(\theta_i)|^2(q_z\xi_0/2)^2, \tag{15}$$

in agreement with standard results from optics.[34] To obtain these results, we have replaced $a_0(q)$ with the two-dimensional equivalent $a_0(q)=2L/\cos\theta_i$, where the surface integral is restricted to the illuminated area of the film. Finally, Eq. (11) is in agreement with that obtained by Albuquerque *et al.*[35] for an optically thick isotropic film [see Eq. (50) in that paper], though our reasoning differs from that employed in the reference.

B. Cross section of the nanoarray

To proceed, we interpret $|u_z(\vec{q},\Delta\omega)|^2$ in Eq. (11) as a thermal average and replace $u_z(\vec{q},\Delta\omega)$ by the associated second-quantized field[22]

$$u_z(x_\perp,t)=\sum_n\int\frac{d^2k}{(2\pi)^2}\left(\frac{\hbar}{2m\omega_{nk}}\right)^{1/2}[a_{nk}\exp(-i\omega_{nk}t) \times u_{nk}(x)+a_{nk}^\dagger\exp(+i\omega_{nk}t)u_{nk}^*(x)] \tag{16}$$

where the $a_{nk}^\dagger(a_{nk})$ are the usual creation (annihilation) operators for mode nk, the $u_{nk}(x)$ are the eigenfunctions, and we have suppressed the index z on the u_{nk} for convenience (recall that $m=\rho\delta$ is the mass per area). The sum and integral are over the states of the periodic nanostructure, summed over the band index n and integrated over the first Brillioun zone in the Bloch wave number k. We have approximated the discrete sum of Bloch wave numbers by an integral. Recall, the $u_{nk}(x)$ are determined in terms of the numerically computed $U_{nk}(x)$ in the unit cell as $u_{nk}(x)=\exp(ikx)U_{nk}(x)$. The normalization is

$$\int dS\, u_{nk}(x)u_{n'k'}^*(x)=\delta_{nn'}(2\pi)^2\delta^2(k-k') \tag{17}$$

and the commutation relations are similarly

$$[a_{nk},a_{n'k'}^\dagger]=\delta_{nn'}(2\pi)^2\delta^2(k-k'). \tag{18}$$

In the usual fashion,[22] we find for the thermal average

$$\langle|u_z(q,\Delta\omega)|^2\rangle_T=\Theta\sum_n\int\frac{d^2k}{(2\pi)^2}\left(\frac{\hbar}{2m\omega_{nk}}\right)\{2\pi\delta(\Delta\omega-\omega_{nk})n_{\Delta\omega}(T)|u_{nk}(q)|^2+2\pi\delta(\Delta\omega+\omega_{nk})\times[n_{\Delta\omega}(T)+1]|u_{nk}(-q)|^2\}, \tag{19}$$

where $n_{\omega_\alpha}(T)$ is the Bose distribution, and the two terms correspond to phonon absorption and emission processes. Equation (19) is a two-dimensional version of the general result for a scalar quantum field.[22]

Provided the illuminated surface S is large, containing many elements in both the x and y directions, the Fourier transform of the Bloch wave function u_{nk} takes on the simple form

$$u_{nk}(q_\perp)=(2\pi/a)^2\delta_N^2(q_\perp-k_\perp)U_{nk}(q_\perp-k_\perp), \tag{20}$$

where

$$\delta_N^2(k)=[a/(2\pi)]^2\sum_{\vec{m}}\exp(-i\vec{k}\cdot\vec{m}a)\approx\sum_{\vec{n}}\delta^2(k-Q_{\vec{n}}) \tag{21}$$

is a lattice delta function and

$$U_{nk}(q)=\int d^2x\exp(-i\vec{q}\cdot\vec{x}_\perp)u_{nk}(x_\perp) \tag{22}$$

is the Fourier transform of the mode shape of a single element of the array. Here, N is the number of elements illuminated by the incident light beam, assumed to be large, and $Q_{\vec{n}}$ are reciprocal lattice vectors.

The normalization requirement Eq. (17) implies $\int_{cell}|U_{nk}(x)|^2=a^2$, the area of a unit cell of the array, so that if the area of an individual element is l^2, we have $U_{nk}\sim(a/l)$. It is therefore convenient to define a dimensionless source strength

$$j_{nk}(q)=(la)^{-1}U_{nk}(q) \tag{23}$$

where for a uniform wave function we have $j_{nk}(q)=1$.

Using Eq. (20), the sum over normal modes indicated in Eq. (19) thus collapses. Substituting into the expression Eq. (11), we find the result for the Brillouin scattering cross section,

$$\left(\frac{d^2\sigma}{d\Omega\, d\omega}\right)_B \approx \frac{N}{2\pi}\sum_n |r(0)\sin\psi\, k_0 q_z l^2 \Delta x_\omega j_{nq}(Q_{\tilde{m}})|^2 \times [\delta(\Delta\omega - \omega_{nq})n_\omega(T) + \delta(\Delta\omega + \omega_{nq})(n_\omega(T)+1)] \quad (24)$$

where the sum is over the subband index n, $\omega=|\Delta\omega|$, and $Q_{\tilde{m}}$ is the unique reciprocal lattice vector satisfying wave vector conservation; i.e., $q=k+Q_{\tilde{m}}$.

The cross section for Brillouin scattering is proportional to the mean square displacement of the ground state of a single oscillator, $\Delta x_\omega^2=\hbar/(2ml^2\omega)$, the geometrical factors, the total number of oscillators N participating in the scattering, and the Bose factors. The scaling behavior of the cross section results from the coherent scattering associated with the N oscillators, each moving with average displacement $\Delta x_M=(\hbar/2Nml^2\omega)^{1/2}$.

One must integrate over an appropriate measurement bandwidth and aperture to obtain a prediction of an observable quantity. We consider here a particularly simple situation: (1) the measurement bandwidth $\delta\omega$ is far greater than the individual linewidths and at the same time far smaller than the bandwidths of the spectrum; and (2) the aperture is large enough to contain all frequencies in the measurement band. In this scenario, the integrations over frequency and solid angle may be estimated in terms of the DOS of the system. For a power P_i incident upon the array, with associated flux $\Phi_i=P_i/(Na^2\cos\theta_i)$, we find the Brillouin scattered power into the anti-Stokes peak for example,

$$P_B(\delta\omega) \approx P_i[r(\theta_i)\sin\psi\, q_z \Delta x_q (l/a)^2 j_q(Q_{\tilde{m}})]^2 \times n_\omega(T)\left(\frac{\cos\theta_i}{\cos\theta_o}\right)\frac{N_o(\omega,\delta\omega)}{N_{tot}} \quad (25)$$

where θ_o is the polar angle of the outgoing wave number, N_{tot} is the total number of elements in the array, and $N_o(\omega,\delta\omega)$ is the number of states with out-of-plane polarization in the measurement band.

We have assumed in obtaining Eq. (25) that a single subband contributes to the cross section, and that the source strength j_q may be assumed constant, assumptions which may be violated depending on the measurement bandwidth and resulting solid angle. If these conditions are violated, Eq. (24) may need to be directly integrated and/or multiple subbands may need to be included.

The Brillouin scattering clearly reveals significant information about the DOS, and more generally the dispersion relations, of the system and is commonly used in this fashion. The scattered power is however also proportional to the mean number $n_{\omega_q}(T)$ (anti-Stokes) or $n_{\omega_q}(T)+1$ (Stokes) of phonons present at temperature T. Therefore, a measurement of the temperature dependence of the Stokes (anti-Stokes) peak would provide direct evidence that the mode q is obeying quantum statistics. Another measurement that has been carried out is the ratio of the Stokes to anti-Stokes peak,[24] which has the advantage of not requiring a temperature scan. Clearly, in either case, measurements are required in the temperature range $k_bT\sim\hbar\omega_q$ to investigate the quantum statistics of mode q.

One final aspect we wish to point out is the effect of fabrication error in the structure. Topological disorder induced by such error reduces the coherence of the Bloch modes and thus the levels of the Stokes and anti-Stokes peaks. Near band edges, however, the Bloch modes of the array are localized by irregularity in the system,[36] and the higher resulting vibration levels partially compensate for the loss of coherence. The mean square displacement level associated with quantum level motion increases as ξ^{-2} as the localization length ξ decreases. Assuming the $q=2|k|\sin\theta/2$ selection rule breaks down as a result of the localization, as in the case of amorphous materials,[37] all q's contribute to the scattering at each angle, and the strength of the scattering is proportional to the area of mode coherence l^2 (l is the coherence length). The cross section for Brillouin scattering will, therefore, be proportional to $(l/\xi)^2 n(\omega)$, where $n(\omega)$ is the density of states. For strong localization of a resonance near a band edge, l/ξ is of order 1, and $n(\omega)$ is of order N, leading to a scattered power of the same order of magnitude as given in Eq. (25). This phenomenon should be observable near the band edges associated with the gaps at 1.5 and 6 GHz for the geometry considered here.

V. DISCUSSION

Here, we consider briefly the order of magnitude of the quantities we have predicted in order to assess whether such measurements are possible in principle. Consider a 1000×1000 array with the geometry as shown in Fig. 1. Using the numerical results from Fig. 2, we find the heat capacity of the sample to be $\sim1.6\times10^{-16}$ J/K at 100 mK. This is certainly small but orders of magnitude larger than in a nanocalorimeter,[2,23] and thus it would seem plausible that the smallness of the heat capacity does not in itself pose a fundamental difficulty.

In the context of Brillouin scattering, we assume the source strength $j_q=1$, a reasonable approximation for a locally rigid-body mode, and assume the polarization-dependent factor $\sin^2\psi=1$. We first note from Eqs. (11) and (24) that provided one is roughly 5° away from the Rayleigh peak (the specular direction) along a diagonal, the level of a Brillouin peak is larger than the Rayleigh wing. To estimate the power level we take the optical wavelength of normally incident light to be 500 nm, $N_o(\omega,\delta\omega)/N=1/4$ (1/4 of the number of modes in a subband), $P_i=100\ \mu$W (a heat load well within the cooling capacity of many current systems), a 1 GHz frequency shift, $\theta=\pi/8$, and $n_{\omega_q}(T)=1$; we then find a Brillouin-scattered power of about 10 photons/s into the Stokes peak. And thus in this case as well, there does not seem to be a fundamental theoretical difficulty in carrying

out the measurement.

Performing such experiments at low temperatures would enable us to observe the quantum statistics obeyed by states involving center-of-mass motion of large numbers of atoms and thus verify that the energy levels of these states are quantized. We have not examined the possibility of employing such a system to explore coherent quantum phenomena, but because the observation of small occupation number states is not out of reach, such an attempt seems promising.

ACKNOWLEDGMENT

The authors gratefully acknowledge the Office of Naval Research for support of this work.

*Electronic address: douglas.photiadis@nrl.navy.mil

[1] L. G. C. Rego and G. Kirczenow, Phys. Rev. Lett. **81**, 232 (1998).
[2] K. Schwab, W. Fon, E. Henriksen, J. M. Worlock, and M. L. Roukes, Physica B **280**, 458 (2000).
[3] A. D. Armour and M. P. Blencowe, Phys. Rev. B **64**, 035311 (2001).
[4] D. W. Carr, W. E. Lawrence, and M. N. Wybourne, Physica B **316-317**, 464 (2002).
[5] I. Tittonen, G. Breitenbach, T. Kalkbrenner, T. Müller, R. Conradt, S. Schiller, E. Steinsland, N. Blanc, and N. F. de Rooij, Phys. Rev. A **59**, 1038 (1999).
[6] A. N. Cleland, D. R. Schmidt, and C. S. Yung, Phys. Rev. B **64**, 172301 (2001).
[7] J. Eisert, M. B. Plenio, S. Bose, and J. Hartley, Phys. Rev. Lett. **93**, 190402 (2004).
[8] S. Bose, K. Jacobs, and P. L. Knight, Phys. Rev. A **59**, 3204 (1999).
[9] A. D. Armour, M. P. Blencowe, and K. C. Schwab, Phys. Rev. Lett. **88**, 148301 (2002).
[10] M. D. LaHaye, O. Buu, B. Camarota, and K. C. Schwab, Science **304**, 74 (2004).
[11] N. W. Ashcroft and N. D. Mermin, *Solid State Physics* (Saunders College, Philadelphia, PA, 1976).
[12] O. L. Lazarenkova and A. A. Balandin, Phys. Rev. B **66**, 245319 (2002).
[13] L. D. Landau and E. M. Lifshitz, *Theory of Elastisity* (Nauka, Moscow, 1965).
[14] B. A. Auld, *Acoustic Fields and Waves in Solids*, 2nd ed. (Robert E. Krieger, Malabar, FL, 1990), Vol. II.
[15] R. D. Mindlin, J. Appl. Mech. **18**, 31 (1951).
[16] G. Kirchhoff, J. Reine Angew. Math. **40**, 51 (1850).
[17] M. Junger and D. Feit, *Sound, Structures, and Their Interaction*, 2nd ed. (MIT Press, Cambridge, MA, 1986).
[18] A. J. Leggett, J. Phys.: Condens. Matter **14**, R415 (2002).
[19] A. O. Caldeira and A. J. Leggett, Phys. Rev. A **31**, 1059 (1985).
[20] D. F. Walls and G. J. Milburn, Phys. Rev. A **31**, 2403 (1985).
[21] D. M. Photiadis, B. H. Houston, J. A. Bucaro, and E. G. Williams, J. Acoust. Soc. Am. **108**, 1027 (2000).
[22] A. L. Fetter and J. D. Walecka, *Quantum Theory of Many Partical Systems* (McGraw-Hill, New York, 1971).
[23] M. L. Roukes, Physica B **263-264**, 1 (1999).
[24] M. Cardona, *Light Scattering in Solids II* (Springer-Verlag, New York, 1982).
[25] D. L. Mills, Y. J. Chen, and E. Burstein, Phys. Rev. B **13**, 4419 (1976).
[26] E. L. Albuquerque, R. Loudon, and D. R. Tilley, J. Phys. C **12**, 5297 (1979).
[27] J. D. Jackson, *Classical Electrodynamics*, 3rd ed. (Wiley, New York, 1999).
[28] R. Loudon, J. Phys. C **11**, 403 (1978a).
[29] K. R. Subbaswamy and A. A. Maradudin, Phys. Rev. B **18**, 4181 (1978).
[30] J. R. Sandercock, Phys. Rev. Lett. **28**, 237 (1972).
[31] S. Mishra and R. Bray, Phys. Rev. Lett. **39**, 222 (1977).
[32] R. Loudon, Phys. Rev. Lett. **40**, 581 (1978).
[33] M. Grimsditch, R. Bhadra, and I. K. Schuller, Phys. Rev. Lett. **58**, 1216 (1987).
[34] E. G. Lean, *Progress in Optics* (North-Holland, Amsterdam, 1973), Vol. 11, pp. 129–135.
[35] E. L. Albuquerque, M. C. Oliveros, and D. R. Tilley, J. Phys. C **17**, 1451 (1984).
[36] S. John, in *Scattering and Localization of Classical Waves in Random Media*, edited by P. Sheng (World Scientific, London, 1990).
[37] R. Shuker and R. W. Gammon, Phys. Rev. Lett. **25**, 222 (1970).